


Article

Plant Tissues and Embryos Biominerals in *Sarcocornia pruinosa*, a Halophyte from the Río Tinto Salt Marshes [†]

Vicenta de la Fuente ^{1,*}, Lourdes Rufo ², Irene Sánchez-Gavilán ¹, Esteban Ramírez ¹, Nuria Rodríguez ³ and Ricardo Amils ^{4,*} 

¹ Departamento de Biología, Universidad Autónoma de Madrid, 28049 Madrid, Spain; irene.sanchezgavilan@estudiante.uam.es (I.S.-G.); esteban.ramirez@uam.es (E.R.)

² Departamento de Farmacia, Universidad Francisco de Vitoria, 28223 Pozuelo de Alarcón, Spain; l.rufo.prof@ufv.es

³ Centro de Astrobiología (INTA-CSIC), 28850 Torrejón de Ardoz, Spain; nrodriguez@cbm.csic.es

⁴ Centro de Biología Molecular Severo Ochoa (CSIC-UAM), Universidad Autónoma de Madrid, 28049 Madrid, Spain

* Correspondence: vicenta.fuente@uam.es (V.d.l.F.); ramils@cbm.csic.es (R.A.); Tel.: +91-497-81-00 (V.d.l.F.); +91-196-45-04 (R.A.)

† The paper is an extended version of our paper published in 1st International Electronic Conference on Mineral Science, 16–21 July 2018.

Received: 10 September 2018; Accepted: 31 October 2018; Published: 5 November 2018



Abstract: Although biomineralization in plants is an important area of research, there is very limited information. In this work, we report the location of Na, K, Ca, Mg and Fe biominerals in *Sarcocornia pruinosa* (Chenopodiaceae), a halophyte species growing in the estuarine area of Río Tinto, an extreme acidic environment. The estuarine soils of the Tinto basin are characterized by slightly acidic pH and high concentrations of ions. They are exposed to Atlantic Ocean tides that contribute to the increase in pH, Na and Mg concentrations. The aim of this work was to characterize the elemental composition and to identify the biominerals detected in cell tissues of *S. pruinosa*. Analytical techniques, such as ICP-MS (Inductively coupled plasma mass spectrometry), XRD and microscopy such as OM (optical microscopy) with histochemical staining, SEM and TEM (scanning and transmission electronic microscopy) coupled with EDX (energy dispersive X-ray) were carried out to analyze the plant tissues of *S. pruinosa* and characterize the detected biominerals. The elemental composition in succulent stems and seeds of *S. pruinosa* showed high values of Na and K followed by Ca, Mg and Fe. The presence of halite, sylvite, weddellite, glushinskite and Fe oxides biominerals in this halophyte species is reported. Our data suggest the importance of vegetation in the biogeochemical cycles in estuarine areas.

Keywords: *Sarcocornia pruinosa*; biominerals; plant cells; seed; embryo; Río Tinto; Biological Absorption Coefficient

1. Introduction

Biomineralization is a term that refers to the processes by which an organism forms minerals. Two different processes have been described: “biologically induced” (precipitation of minerals as a result of the interaction of the organisms and the environment) and “biologically controlled” (the cells control crystal formation). This last can lead to the production of extra-, inter- or intracellular minerals [1]. Plants are reported to be able to produce biominerals in most organs and tissues, with the most common being calcium biominerals, mainly as oxalates and carbonates, but sulphates and phosphates have been also observed. Other minerals known to be formed by plants are

amorphous silica or magnesium oxalate [2–6]. Also, Fe biomineralization such as jarosite and Fe-oxides (ferrihydrite, hematite and spinel phases) were thoroughly studied in the grass *Imperata cylindrica* growing on the Río Tinto and also under controlled hydroponic cultures [7,8]. Other authors also highlight the impact of biomineralization processes in plants that grow in environments with a high presence of metals resulting from biogeochemical cycles [9,10].

Sarcocornia pruinosa Fuente, Rufo & Sánchez Mata is a succulent halophyte from the *Sarcocornia* genus (Chenopodiaceae family) recently described for European Atlantic estuarine coastal salt marshes (France, Portugal and Spain). It is a perennial woody subshrub up to 50 cm tall with woody, terete and erect main branches followed by succulent erect or ascending, secondary stems, characterized by reduced opposite amplexicaule scale like leaves, fused to the stem forming a collar like segment, and by spicate inflorescences with opposite three flowered cymes that contain reduced flowers [11].

S. pruinosa occurs in low- and mid-intertidal zones subjected to regular and partial flooding by daily tides in the European Atlantic saltmarshes from southern Spain to southern France. Río Tinto is located in the southwest of the Iberian Peninsula (Huelva province) and its last section, together with the Río Odiel, forms an estuary located in the city of Huelva. There is extensive literature that justifies the extreme and unique character of Río Tinto due to its acidity (average pH: 2.3) which remains constant along the length of its first 80 km, and the high concentration of heavy metals (Fe, Cu, Zn, As, Cr, Pb among others) detected in its waters. Studies of sediments and soils along the river show that these characteristics are also present. Estuarine soils have been described as ranging from extremely acidic to slightly alkaline and slightly saline. They contain high concentration of S and Fe together with Na, Mg, P, Cu and Zn. Mineralogy of these soils is composed mainly of quartz, phyllosilicates (kaolinite and illite), Ca–Na feldspars, K-feldspars, dolomite and calcite [12,13].

The flora of this territory corresponds to halophyte vegetation, in particular, to perennial graminoids communities and succulent Chenopodiaceae shrubs. This last includes *S. pruinosa*, which constitutes the main biomass of these succulent suffruticose communities subjected to daily tides influence.

As a halophyte, *S. pruinosa* grows and reproduces in saline environments (salt concentration ≥ 200 mmol/L) [14]. To maintain a positive turgor pressure, halophytes must adjust osmotically, and thus their cells should have a greater total solute concentration than the soil solution. In order to achieve this, halophytes accumulate saline ions (in dicotyledonous mainly Na^+ and Cl^-) in their vacuoles and organic solutes in their cellular cytoplasm. Therefore, a high concentration of salts is likely and this could lead to the formation of different biominerals.

On the other hand, it has been pointed out that the adaptive capacity of halophytes plants may be of use in the phytoremediation of areas polluted with heavy metals since they are able to accumulate ions and to cope with oxidative stress [15]. Other applications of potential interest are their use as food or forage in areas with high salinity, as has been observed in other succulent genera of the Chenopodiaceae family [16]. In addition, the genus *Sarcocornia* along with other halophytes have long been valued in the traditional manufacture of soaps or in the use of salts present in their ashes [17].

The aim of this work was to characterize the elemental composition, describe their biomineral morphological characteristics and identify their distribution in different organs and tissues of the halophytic species of *S. pruinosa* in their natural habitats, using different and complementary analytical methodologies.

2. Materials and Methods

2.1. Plant Material

Complete individuals of *S. pruinosa* were collected directly from the riverside communities of Río Tinto, in high salt marsh (San Juan del Puerto, UTM 29SPB9331) and low salt marsh areas (Monumento a Colón, UTM 29SPB3820) (Huelva, Spain), selecting the best preserved and with similar size. Samples

were stored at 4 °C until being deep frozen upon arrival at the laboratory. Three wild samples were selected for elemental analysis from each locality.

2.2. X-ray Diffraction Analysis

X-ray analysis were carried out in the Interdepartmental Research Service (SIID) of Universidad Autónoma de Madrid using a Siemens-D5000 (Siemens AG, Karlsruhe, Germany), diffractometer with Cu K α (8.04 keV) radiation and a SOL-X detector provided by Bruker (Billerica, MA, USA).

Samples of *S. pruinosa* were analyzed using the unoriented powder method. The software used to draw the diffractogram and search for crystalline phases was the PANalytical X'Pert HighScore Plus (version 3.0). Crystallographic patterns from the PDF-4 base of the ICDD (International Diffraction Data Center) were used to determine the different minerals present on the plants.

2.3. Elemental Analysis

Succulent stems of three samples of each locality (a total of six samples) were selected, washed with distilled water and dried in an oven at 75 °C for 24 h. Seeds of a sample of *S. pruinosa* of San Juan del Puerto salt marsh were separate from the rest of the pericarp and flowers under a microscope. Dried samples were powdered for homogenization.

The digestion of the samples followed the standardized protocol for multi-elemental analysis of plant material described by Zuluaga et al. [18]. A portion of approximately 500 mg of powdered samples were digested at high pressure in a mixture of 8 mL of HNO₃ 65% and 2 mL of H₂O₂ 30% in a MLS Ethos 1600 URM Milestone microwave digester (Milestone Srl, Sorisole (BG), Italy) The samples were then analyzed by ICP-MS using an ELAN-6000 PE-Sciex (PE Sciex, Toronto, ON, Canada) instrument for Na, Ca, Mg, K, Mn, Fe, Ni, Cu, Zn, As Pb, Ba and Sr content. The ICP-MS technique used has an inherent error of 15%.

2.4. Histochemical Staining of Fe with Prussian Blue Stain Formation

For the histochemical staining of iron, the protocol described by Roschztardt et al. [19] based on Prussian Blue stain or ferrocyanide reaction has been followed. Plant sections were infiltrated with volumes of 4% (v/v) HCl and 4% (w/v) K-ferrocyanide (Perls stain solution) for 15 min and incubated for 30 min at room temperature. Then samples were washed with distilled water and photographed with an Olympus SC30 camera attached to an Olympus SZX10 stereomicroscope (Tokyo, Japan).

2.5. Scanning Electron Microscopy (SEM)

Succulent stems, leaves and embryos of *S. pruinosa* were analyzed by SEM complemented with an energy dispersive X-ray analyzer (EDX) following the methodologies previously described in Rodríguez et al. 2005; Amils et al. 2007 and Fuente et al. 2012 [20–22].

2.6. Transmission Electronic Microscopy (TEM)

Sections of plant tissues and embryos of approximately 1 mm³ were fixed in the Electron Microscopy Service of Centro de Biología Molecular Severo Ochoa (CBMSO) with the method described in Fuente et al. 2016 and 2017 [7,10]. Samples were observed in the same service with a JEM-1010 transmission electron microscope and in the Centro Nacional de Microscopía Electrónica de Madrid with a JEM 2000FX electron microscope (JEOL, Tokyo, Japan) operated at 200 kV, coupled with an energy dispersive X-ray microanalysis instrument LINK ISIS 300 (Oxford Instruments, Oxford, UK).

3. Results

3.1. X-ray Diffraction Analysis

We present data of two representative samples located in a high salt marsh area. In the first diffractogram, the highest intensity diffraction peaks (Figure 1A) correspond to halite (NaCl) and calcium oxalate dihydrate weddellite ($C_2CaO_4 \cdot 2H_2O$).

In the second spectrum, halite (NaCl), sylvite (KCl) and weddellite ($C_2CaO_4 \cdot 2H_2O$) have been detected. The peak of lower intensity corresponds to magnesium oxalate dihydrate glushinskite ($C_2MgO_4 \cdot 2H_2O$) (Figure 1B). Peaks of lower intensity but not detected by other techniques have not been taken into account.

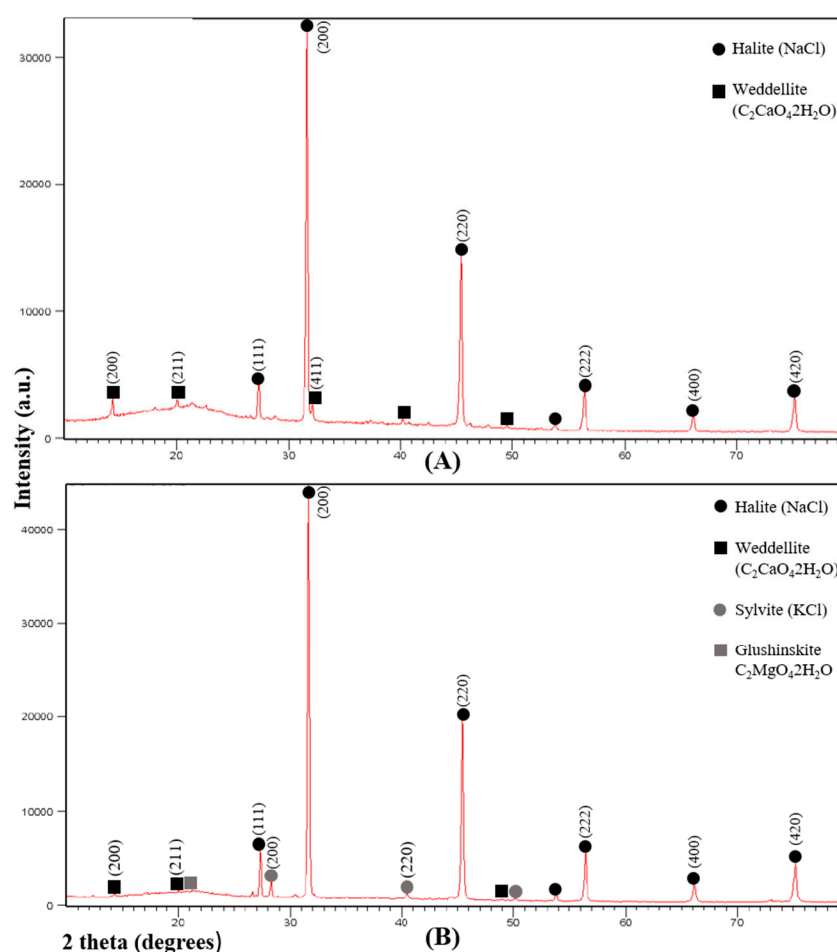


Figure 1. Representative X-ray diffraction spectra of succulent stems of *S. pruinosa*. (A) Halite and weddellite. (B) Halite, weddellite, sylvite and glushinskite. Numbers in parentheses in the most intense peaks refer to the crystallographic planes (*hkl*).

3.2. Elemental Composition

The Río Tinto soils in which *S. pruinosa* is found are exposed to the daily tidal flow. The characteristics of the estuarine soils in the Río Tinto basin have been described with a mean pH of 6.3, slightly acidic and an average electrical conductivity of 6.22 dS/cm. The analysis of the elemental composition of the soil shows high concentrations of S, Fe, Na, Mg and P. They also present high concentration values for Cu, Zn, Pb and As [13].

As for *S. pruinosa* samples, most of the elements measured by ICP-MS in succulent stems had the normal ranges for vascular plants [23]. The highest measured concentration corresponded to Na, with values over 10,000 mg/kg for seeds and over 61,000 mg/kg for succulent stems. The values

obtained for the macronutrients Mg, Ca and K were over 4000 mg/kg. The data for seeds followed a similar pattern, highlighting the values of Ca, Mg and K. The other element with high concentrations was Fe with 418 mg/kg for seeds and mean values of 245 mg/kg for succulent stems (Table 1).

The values obtained for the micronutrients Mn, Ni and Zn and the toxic elements As and Pb were found in normal ranges, while Cu showed high concentrations for both, seeds and succulent stems (Table 1). The Biological Absorption Coefficient (BAC) values for Na, Mg and K show that *S. pruinosa* actively absorbs and accumulates these elements in its tissues (BAC > 1). Our analysis confirms the results already described for the Río Tinto flora [24]. All raw data is collected in Table S1 of the Supplementary Materials.

Table 1. Elemental composition of the soils and the seed and succulent stem of *Sarcocornia pruinosa* analyzed by ICP-MS, and the correspondent BAC values. Soil data have been extracted from the data set of Rufo et al. [13]. A sample of soil of the sampled areas (salt marsh interior and end of the river) has been selected. All data are expressed in mg/kg. M: mean; SD: Standard deviation; nd: under the detection limit. Number of samples: A (seed): n = 1; B (soil): n = 1; B (succulent stems): n = 3; C (soil): n = 1; C (succulent stems): n = 3.

Sample	Na	Ca	Mg	K	Mn	Fe	Ni	Cu	Zn	As	Pb	Ba	Sr
A Seed	16,612	7645	6231	6865	13.7	418	5.32	191	56.3	2.48	5.30	6.06	450
B (Soil)	9737	1293	6516	4053	891	39,962	24.8	594	481	82.0	178	37.4	16.9
B (M)	75,160	4591	6357	7005	33.5	377	4.92	61.8	59.2	2.82	5.24	5.99	29.7
SD	42,021	2195	754	1466	21.3	334	0.68	84.8	51.4	3.15	5.96	7.82	25.5
BAC (M)	7.72	3.55	0.98	1.73	0.04	0.01	0.20	0.10	0.12	0.03	0.03	0.16	1.76
SD	4.32	1.70	0.12	0.36	0.02	0.01	0.03	0.14	0.11	0.04	0.03	0.21	1.51
C (Soil)	6687	5813	4591	1729	136	47,319	13.1	830	1355	713	566	221	169
C (M)	47,055	6329	6539	10,137	15.36	113.6	1.94	66.51	26.25	0.01	nd	3.15	37.88
SD	2294	512	3213	640	3.16	79.5	0.30	6.47	0.86	0.00	-	0.48	2.71
BAC (M)	7.04	1.09	1.42	5.86	0.11	0.002	0.15	0.08	0.02	0.14×10^{-4}	-	0.01	0.22
SD	0.34	0.09	0.70	0.37	0.02	0.002	0.02	0.01	0.0006	0.00	-	0.002	0.02

3.3. Microscopic Analysis

3.3.1. Stems and Leaves

The accumulation of biominerals in *S. pruinosa* has been studied under SEM microscopy in the different visible tissues in the transverse and longitudinal sections of their stems (epidermis, parenchyma and vascular bundle, Figure 2A–D). The greatest accumulation and variety of biominerals are found in the parenchymal tissue, followed by the vascular bundle and finally the epidermis, sometimes with large crystalline structures.

In the outermost layer of the stems, the epidermis, sodium and chlorine crystals predominate (Figures 2A and 3A and Appendix A). Less frequently in this layer have observed structures been dominated by calcium crystals with chlorine and sodium (Appendix A). In the parenchyma of the succulent stems, the main crystals are of NaCl (Figure 3B), mixtures of K, Na, Cl crystals with other elements (Figure 3C), and the possible presence of tetragonal bipyramid shape or cubic crystals made mainly of Ca crystals (Figure 4A,B). Mg mineralizations have been found mostly in the parenchymal cells of the transverse sections of stems with flowers (Figures 2C and 4C and Appendix A). Some particles formed by a mixture of Fe, S, Na, Cl, Si, Al, Mg and K have been less frequently observed in the walls of the parenchymal cells of the floriferous stems (Appendix A). In the vascular bundle, mainly crystalline structures are found collapsing the vessels in mixtures with Na, K and Cl as major elements (Figure 3D and Appendix A). Frequent predominant Ca mineralizations can be also found with other salts covering the ducts of the vascular bundles (Figures 2D and 4D and Appendix A).

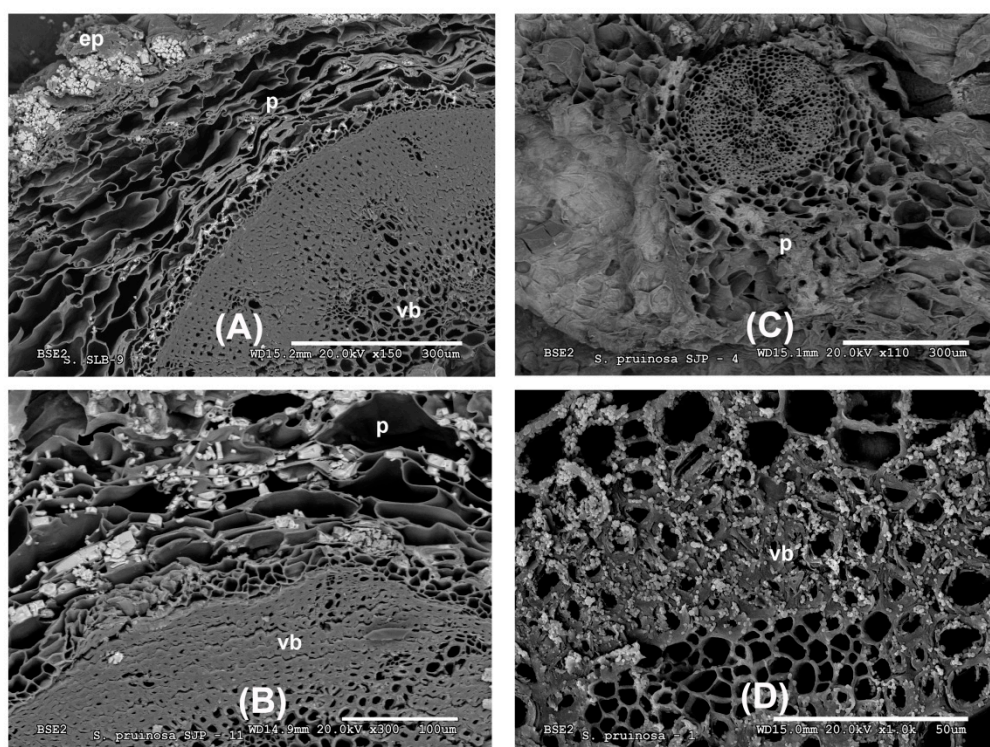


Figure 2. Representative SEM images of the tissue location of Na, K, Mg and Ca biominerals in *S. pruinosa*. (A) Stem cross section with Na and K salts. (B) Major salts of NaCl in parenchyma of transverse section of stem. (C) Location of Mg in parenchyma of flowering stem. (D) Vascular bundle showing abundant Ca crystals. Symbology: ep = epidermis; p = parenchyma; vb = vascular bundle.

3.3.2. Seeds and Embryos

The use of Prussian Blue staining on stems, leaves, flowers, fruits and seeds of the plant indicate a heterogeneous distribution of iron in these tissues. Representative samples of cuts made in the stem and in the seeds extracted from the stem reveal the absence of epidermis staining and are scarce in parenchyma and vascular vessels. However, intense staining was observed in the two cotyledons included within the seed (Figure 5A). No staining was observed in the pericarp and in the trichomes of the seeds. Elemental mapping spectra in the longitudinal section of seed performed with SEM showed a constant proportion of different biomineral elements predominant throughout the embryo (K, Cl, Na, Ca, and Fe) (Figure 5B,C). However, higher peaks were observed for Ca in the seed coat (Figure 5B,C). For this element, crystalline nanoparticles have been found in the longitudinal sections of TEM embryos (Figure 5D,E). With intense peaks observed in the EDX analysis (Figure 5F).

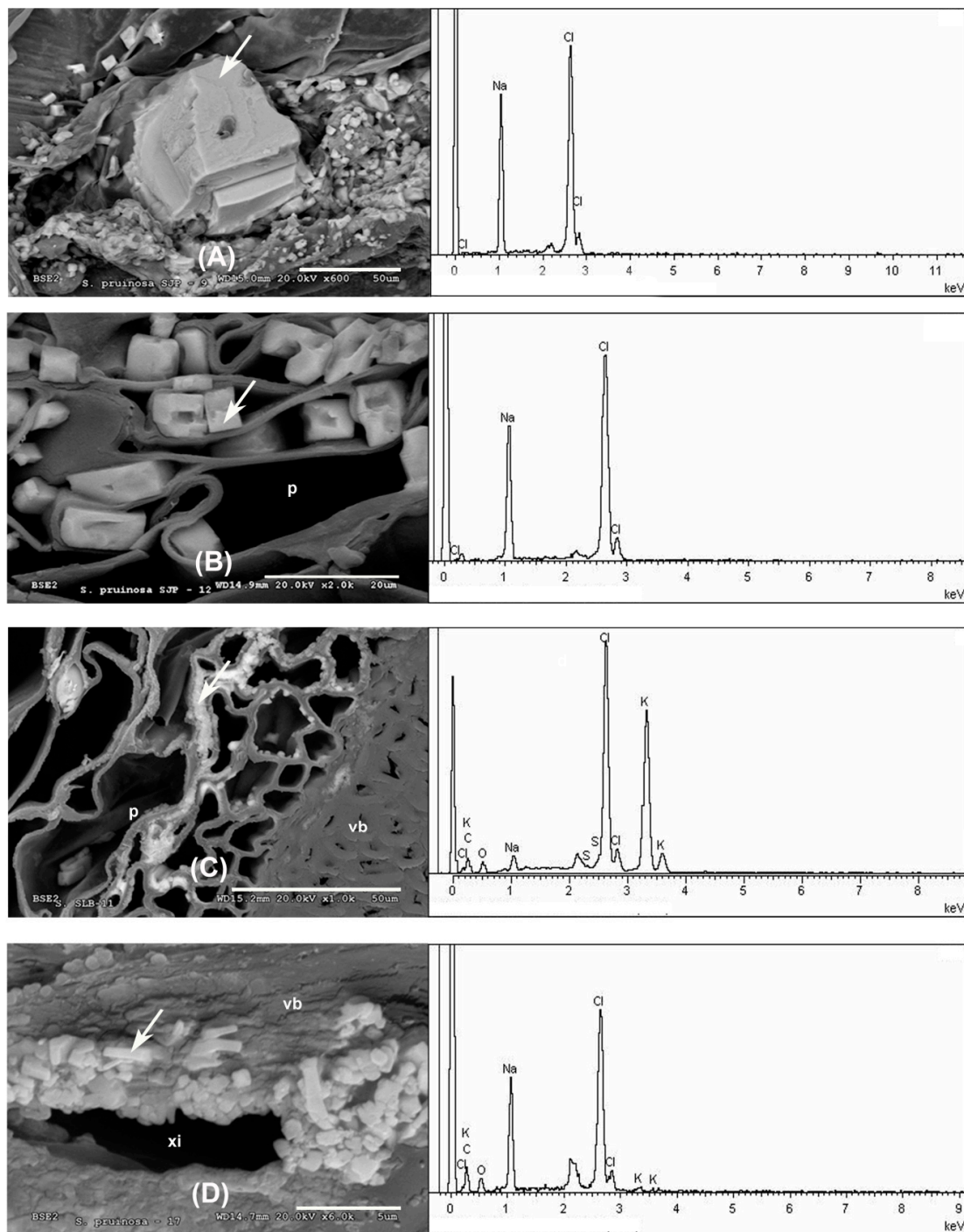


Figure 3. Representative SEM images of Na and K biominerals in *S. pruinososa*. (A) Details of NaCl crystals in the epidermis. (B) Major salts of NaCl in parenchyma of transverse section of stem. (C) Detail of KCl salts in the parenchyma. (D) Xylem of floriferous stem collapsed by crystals of K, Cl and Na. EDX spectra to the right of each section corresponds to the analyzed spot represented by the white arrow. Symbology: ep = epidermis; p = parenchyma; vb = vascular bundle; xi = xylem.

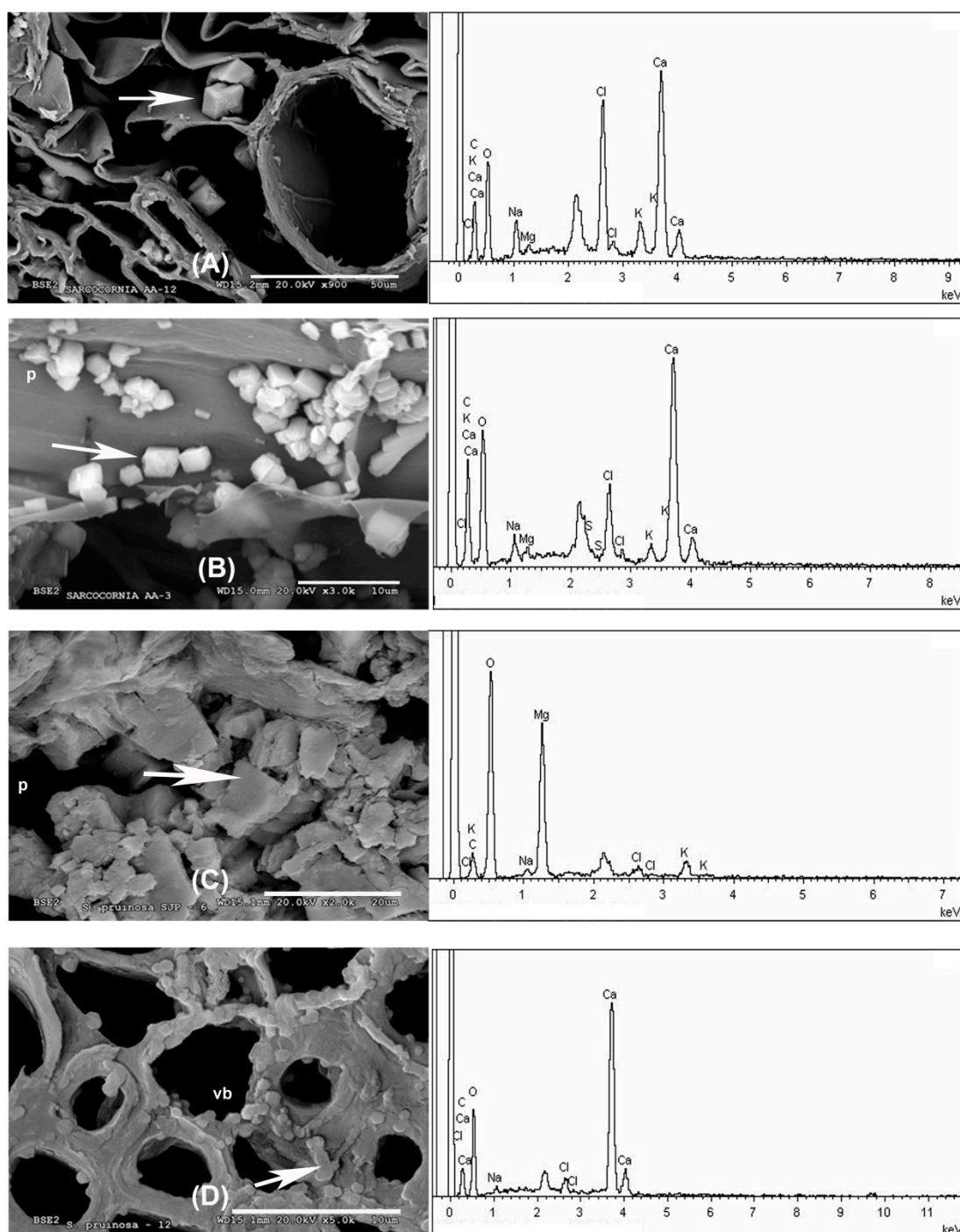


Figure 4. SEM images representative of Ca and Mg biominerals in succulent stems of *S. pruinosa*. (A) Cubic structures of Ca in parenchyma. (B) Ca crystals in the parenchyma cell walls in longitudinal section. (C) Detail of Mg in the parenchyma. (D) Detail of the Ca crystals. EDX spectra to the right of each section corresponds to the analyzed spot represented by the white arrow. Symbology: p = parenchyma; vb = vascular bundle.

The accumulation of iron can also be observed in embryos by OM (Optical Microscopy), SEM and TEM. Iron is localized in the root and in both cotyledons, preferably in the embryonic cells that later become the initial central cylinder (Figure 5A,G,I). Electro-dense precipitates of iron can be observed by TEM embryo cells of radicle, and more exactly in the cell wall and in the root cap. They are also found in the cotyledon embryonic cells (Figure 5G,I). In this case, the correspondent spectra only detected

the presence of iron oxides in nanometers amorphous particulates, of approximately 100 nm sizes. All these iron biominerals are constant and abundant along the cell walls of the embryos, especially concentrated in the radicular edges. EDX associated with the TEM equipment shows high peaks of Fe (Figure 5).

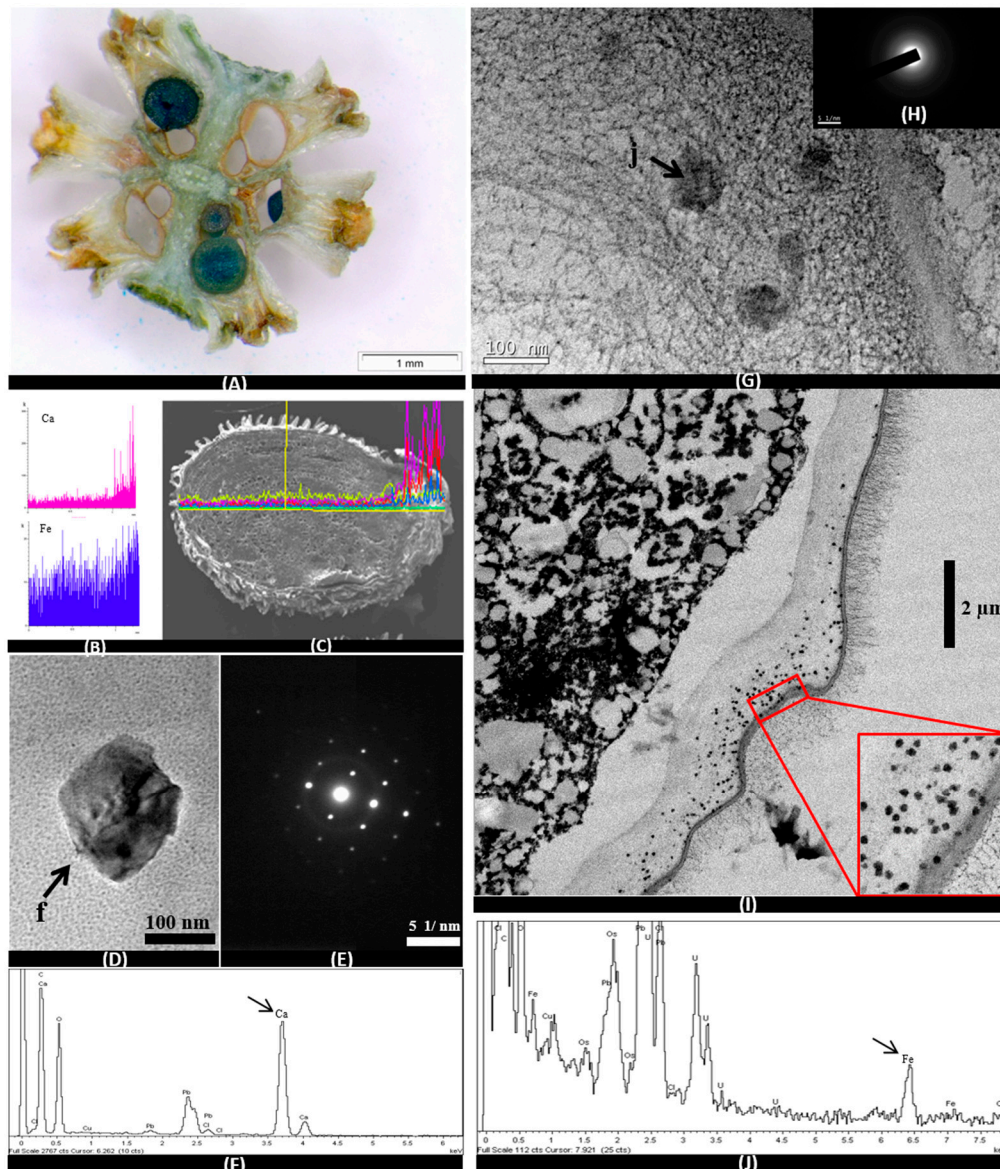


Figure 5. Images OM (A), SEM (C), TEM (D, E, G, H and I), SEM-EDX spectra (B) and TEM-EDX spectra (F and J) in embryos of *S. pruinosa*. (A) Cross section of floriferous stem with embryos completely dyed blue by Prussian Blue staining. (B) Representative Ca and Fe EDX spectra of embryo mapping in the longitudinal section of the seed. (C) Longitudinal section of the seed with the mapping from the spectra. (D) Crystal of Ca in cells of the radicle. (E) Electro diffraction pattern of calcium crystal. (F) EDX spectrum of the Ca crystal analyzed in part D of this figure. (G) Detail of nanometric particles of Fe at the edges of the embryo radicle. (H) Pattern of the Fe particles without diffraction. (I) Radicle edge with iron particles. (J) EDX spectrum of the Fe particles analyzed in part G of this figure.

4. Discussion

S. pruinosa, a halophyte species typical of the Atlantic marsh ecosystems of Río Tinto, shows great capacity to accumulate different elements in relation to the soil where it grows. The nutrient concentrations measured in *S. pruinosa* present similar ranges to those previously published for other halophytes that grow in this environment [24].

In the Tinto River salt marshes, Na, Ca, K and Mg are the ions that have higher concentrations inside the plant. These observations also correlate with the ionic values found in other species of Chenopodiaceae close to the genus *Sarcocornia* [25]. However, the dominance of each of the four elements in the plant tissues will depend on the combination of several factors such as soil materials or the differing degrees of salinity degree produced by the tides [26], and it is not a trivial task to provide a specific order of predominance of these macro and micronutrients. On the other hand, Fe concentration must be highlighted, as it is has a significant presence both in succulent stems and in seeds.

The BAC values show that *S. pruinosa* follows an accumulation strategy for Na similar to other known succulent halophytes [14]. Other elements such as Ni, Cu, Zn, As and Pb are below one, which could be associated with an exclusion strategy, which has been described as the most common among the flora of Río Tinto [24].

A semiquantitative XRD analysis of the major crystal phases in samples of *S. pruinosa* consisted of halite, weddellite, sylvite and glushinskite. These data are congruent with the crystal structures detected by SEM in the different and representative sections of the leaves and floriferous and non-floriferous stems (Figures 2–4), where Na, Ca, K and Mg crystals have more frequently been found.

The accumulation of salts, especially Na in this halophyte species, occurs in the cell vacuoles of virtually all tissues, although with greater presence in the tissues of the spongy parenchyma, which is a strategy of the plant to adapt to growing in soil media with high salt concentrations. Osmotic equilibrium at the cellular level is accomplished with K, whose concentrations are much higher than those needed by other species. On the other hand, the accumulation of Na occurs in biologically less active tissues and cells, such as the xylem vascular bundles of flowering stems, and spongy parenchyma cells next to the epidermis. The concentration of halite and sylvite constitutes a biological process controlled by this species and we suggest that their storage in inactive forms may be a way to exclude ions that are toxic at a cellular level such as Na. In the case of K, given its low concentration, it can be a reservoir.

Ca oxalate biominerals (the mono-, di-, and tri-hydrates of $\text{Ca}(\text{C}_2\text{O}_4)$), are the most common family of organic minerals in natural environments and the accumulation and precipitation patterns of Ca and Mg are more species-specific than substrate-affected [5]. Ca oxalate biomineralization is a good example of a biologically controlled process [27–29], as the chemical nature and crystal type as well as their location within the plant body are under strict genetic control [6]. Weddellite, $\text{C}_2\text{CaO}_4 \cdot 2\text{H}_2\text{O}$, is the biomineral found in greater proportion in this species as it is the most common of all in nature. The presence of this oxalate in the embryo is evidence of the genetic control of the species as it facilitates the transport and subsequent accumulation of calcium in crystalline form, as observed (Figure 5D).

Together with weddellite, we find in a smaller proportion the dihydrated oxalate $\text{C}_2\text{MgO}_4 \cdot 2\text{H}_2\text{O}$. This biomineral was also detected in the Cactaceae species *Opuntia ellisiana*, associated with whewellite and opal, which was the first evidence of the presence of this oxalate in plants [5].

We would like to highlight the first results of biominerals found in this species and in other halophytes of the Chenopodiaceae family. A semiquantitative XRD analysis of the major crystal phases in samples of *S. pruinosa* consisted of halite, weddellite, sylvite and glushinskite. These data are congruent with the crystal structures detected by SEM in the different and representative sections of the leaves and floriferous and non-floriferous stems, where Na, Ca, K and Mg crystals were found most frequently.

Iron oxides were not detected by XRD probably due to their low concentrations or to the amorphous state in which these minerals are found as cell wall components. However, complementary

techniques allowed the presence of Fe in *S. pruinosa* tissues to be visualized, especially in seeds. With the use of the histochemical Prussian Blue stain, we were able to identify the presence of Fe in all the embryonic tissue cells. SEM images often showed the presence of Fe in the cotyledons and radicle, as reflected in the mapping images presented (Figure 5B,C). At the cellular level, the presence of Fe was detected by TEM and HRTEM (High-resolution transmission electron microscopy) and corresponds to the high concentration of Fe aggregates detected by EDX in the root cap tip and root axis. The XRD spectrum of those nanoparticles found in the embryonic tissue cell walls (Figure 5I), in which Fe was detected together with the C and O of the cell wall constituents (Figure 5J), suggests that they correspond to amorphous iron oxides. In other species such as the grass *Imperata cylindrica* iron oxides were detected embedded in an amorphous silica matrix, and plant incineration allowed the crystallinity of the Fe deposits to be detected [7]. It is probable that the higher presence of Fe nanoparticles found in the root embryonic tissues is due to the positive gravitropism that characterizes the plant roots.

This work is a complete characterization of the biominerals present in one of the most representative species of the saline ecosystems of Río Tinto. Our data reveal the mineral composition of *S. pruinosa* and the importance that its use can have in different nutritional and biotechnological applications.

Supplementary Materials: The following are available online at <http://www.mdpi.com/2075-163X/8/11/505/s1>, Table S1: *Sarcocornia pruinosa* ICP calculated for Na, Ca, Mg, K, Mn, Fe, Ni, Cu, Zn, As, Pb, Ba and Sr from plant concentrations of these elements. Data expressed in mg/kg.

Author Contributions: For research articles with several authors, a short paragraph specifying their individual contributions must be provided. The following statements should be used “Conceptualization, V.F. and R.A.; Methodology, V.F., R.A., L.R., I.S.-G., E.R., N.R.; Validation, E.R., and L.R.; Formal Analysis, V.F., R.A., L.R., I.S.-G., E.R., N.R.; Investigation, V.F., R.A., L.R., I.S.-G., E.R., N.R.; Resources V.F., R.A.; Writing—Original Draft Preparation, V.F.; Writing—Review & Editing, R.A., V.F.

Funding: This research was funded by the Ministerio de Economía y Competitividad (MEC, Spanish Government).grant number CGL2015 66-242 R.

Conflicts of Interest: The authors declare no conflict of interest.

Appendix A

Table A1. Major biomineral elements and location of *Sarcocornia pruinosa* with SEM Image Analysis and EDX Spectrum.

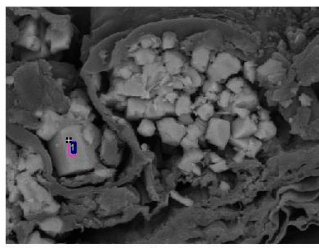
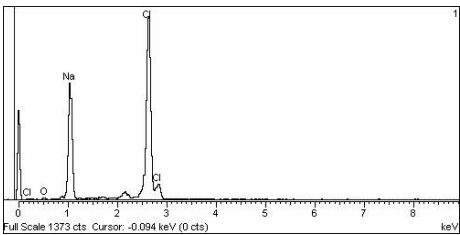
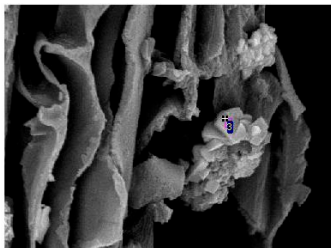
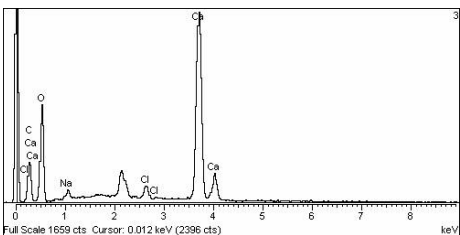
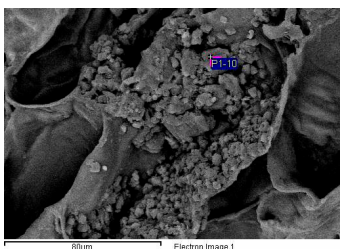
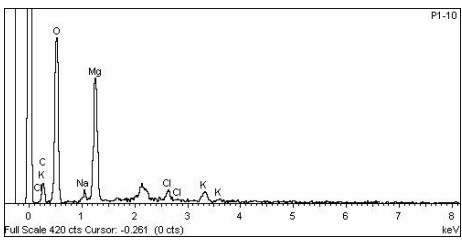
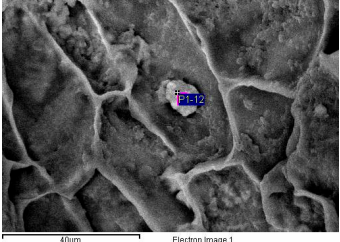
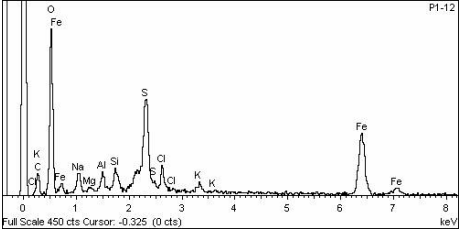
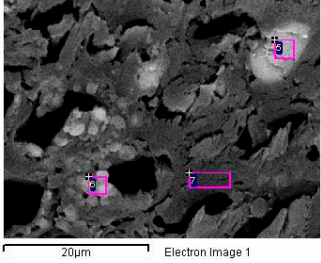
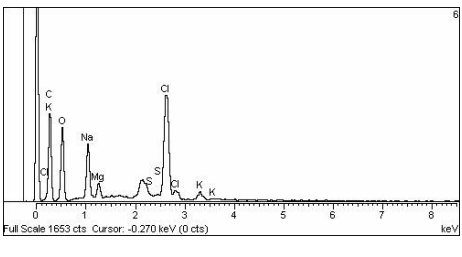
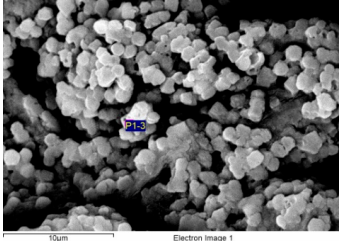
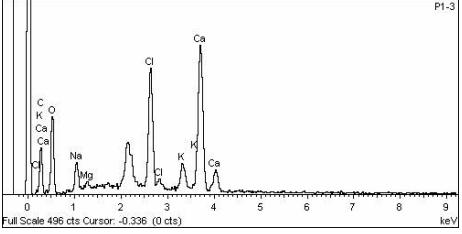
Major Biomineral Elements and Location	SEM Image Analysis	EDX Spectrum
1 Cl > Na —Epidermis of transversal section of non-floriferous stem		
2 Ca > Cl > Na —Epidermis of longitudinal section of non-floriferous stem		

Table A1. Cont.

Major Biomineral Elements and Location	SEM Image Analysis	EDX Spectrum
3 Mg > K > Cl > Na —Parenchyma of transversal section of floriferous stem		
4 Fe > S > Na > Cl > Si > Al > Mg > K —Epidermis of longitudinal section of non-floriferous stem		
5 Cl > Na > Cl > K > Mg > S —Epidermis of longitudinal section of non-floriferous stem		
6 Ca > Cl > K > Na > Mg —Vascular bundle of non-floriferous stem		

References

- Lowenstam, H.A. Mineral formed by organisms. *Science* **1981**, *211*, 1126–1131. [[CrossRef](#)] [[PubMed](#)]
- Franceschi, V. Calcium oxalate in plants. *Trends Plant Sci.* **2001**, *6*, 331. [[CrossRef](#)]
- Dietrich, D.; Hinke, S.; Baumann, W.; Fehlhäber, R.; Bäucker, E.; Rühle, G.; Wienhaus, O.; Marx, G. Silica accumulation in *Triticum aestivum* L. and *Dactylis glomerata* L. *Anal. Bioanal. Chem.* **2003**, *376*, 399–404. [[CrossRef](#)] [[PubMed](#)]
- Lins, U.; Barros, C.; da Cunha, M.; Miguens, F.C. Structure, morphology, and composition of silicon biocomposites in the palm tree *Syagrus coronata* (Mart.) Becc. *Protoplasma* **2002**, *220*, 89–96. [[CrossRef](#)] [[PubMed](#)]
- Monje, P.V.; Baran, E.J. Evidence of formation of glushinskite as a biomineral in a *Cactaceae* species. *Phytochemistry* **2005**, *66*, 611–614. [[CrossRef](#)] [[PubMed](#)]
- He, H.; Veneklaas, E.J.; Kuo, J.; Lambers, H. Physiological and ecological significance of biomineralization in plants. *Trends Plant Sci.* **2014**, *19*, 166–174. [[CrossRef](#)] [[PubMed](#)]
- Fuente, V.; Rufo, L.; Juárez, B.H.; Menéndez, N.; García-Hernández, M.; Salas-Colera, E.; Espinosa, A. Formation of biomineral iron oxides compounds in a Fe hyperaccumulator plant: *Imperata cylindrica* (L.) P. Beauv. *J. Struct. Biol.* **2016**, *193*, 23–32. [[CrossRef](#)] [[PubMed](#)]

8. De Giudici, G.; Pusceddu, C.; Medas, D.; Meneghini, C.; Gianoncelli, A.; Rimondi, V.; Podda, F.; Cidu, R.; Lattanzi, P.; Wanty, R.; et al. The role of natural biogeochemical barriers in limiting metal loading to 312 a stream affected by mine drainage. *Appl. Geochem.* **2017**, *76*, 124–135. [[CrossRef](#)]
9. Medas, D.; De Giudici, G.; Pusceddu, C.; Casu, M.A.; Birarda, G.; Vaccari, L.; Gianoncelli, A.; Meneghini, C. Impact of Zn excess on biomineralization processes in *Juncus acutus* grown in mine polluted sites. *J. Hazard. Mater.* **2017**. [[CrossRef](#)] [[PubMed](#)]
10. Fuente, V.; Rufo, L.; Rodríguez, N.; Franco, A.; Amils, R. Comparison of iron localization in wild plants and hydroponic cultures of *Imperata cylindrica* (L.) P. Beauv. *Plant Soil* **2017**, *418*, 25–35. [[CrossRef](#)]
11. Fuente, V.; Oggerin, M.; Rufo, L.; Rodríguez, N.; Ortuñez, E.; Sánchez-Mata, D. A micromorphological and phylogenetic study in *Sarcocornia* A.J. Scott (Chenopodiaceae) in Iberian Peninsula. *Plant Biosyst.* **2013**, *147*, 158–173. [[CrossRef](#)]
12. Rufo, L.; Rodríguez, N.; Amils, R.; Fuente, V.; Jiménez-Ballesta, R. Surface geochemistry of soils associated to the Tinto River (Huelva, Spain). *Sci Total Environ.* **2007**, *378*, 223–227. [[CrossRef](#)] [[PubMed](#)]
13. Rufo, L.; Rodríguez, N.; Fuente, V. Chemical and mineralogical characterization of the soils of the main plant communities of the ‘Río Tinto’ basin. *Schironia* **2010**, *9*, 5–12.
14. Flowers, T.; Colmer, T.D. Salinity tolerance in halophytes. *New Phytol.* **2008**, *179*, 945–963. [[CrossRef](#)] [[PubMed](#)]
15. Lutts, S.; Lefèvre, I. How can we take advantage of halophyte properties to cope with heavy metal toxicity in salt-affected areas? *Ann. Bot.* **2015**, *115*, 09–528. [[CrossRef](#)] [[PubMed](#)]
16. Khan, M.A.; Gul, B. *Arthrocnemum macrostachyum*: A potential case for agriculture using above seawater salinity. *Prospect. Saline Agric.* **2002**, *37*, 353–364. [[CrossRef](#)]
17. Lagasca, M. *Memoria Sobre Las Plantas Barrileras de España*; En la Imprenta Real: Madrid, Spain, 1817; pp. 1–84.
18. Zuluaga, J.; Rodríguez, N.; Rivas-Ramirez, I.; Fuente, V.; Rufo, L.; Amils, R. An improved semi-quantitative method for elemental analysis of plants using inductive coupled plasmamass spectrometry. *Biol. Trace Elem. Res.* **2011**, *144*, 1302–1317. [[CrossRef](#)] [[PubMed](#)]
19. Roschttardt, H.; Conéjero, G.; Curie, C.; Mari, S. Identification of the endodermal vacuole as the iron storage compartment in the *Arabidopsis* embryo. *Plant Physiol.* **2009**, *151*, 1329–1338. [[CrossRef](#)] [[PubMed](#)]
20. Rodríguez, N.; Menéndez, N.; Tornero, J.; Amils, R.; Fuente, V. Internal iron biomineralization in *Imperata cylindrica*, a perennial grass: chemical composition, speciation and plant localization. *New Phytol.* **2005**, *165*, 781–789. [[CrossRef](#)] [[PubMed](#)]
21. Amils, R.; Fuente, V.; Rodríguez, N.; Zuluaga, J.; Menéndez, N.; Tornero, J. Composition, speciation and distribution of iron minerals in *Imperata cylindrica*. *Plant Physiol. Biochem.* **2007**, *45*, 335–340. [[CrossRef](#)] [[PubMed](#)]
22. Fuente, V.; Rodríguez, N.; Amils, R. Immunocytochemical analysis of the subcellular distribution of ferritin in *Imperata cylindrica* (L.) Raeuschel, an iron hyperaccumulator plant. *Acta Histochem.* **2012**, *114*, 232–236. [[CrossRef](#)] [[PubMed](#)]
23. Brooks, R.R. *Plants that Hyperaccumulate Heavy Metals: Their Role in Phytoremediation, Microbiology, Archaeology, Mineral Exploration and Phytomining*, 2nd ed.; CAB International: New York, NY, USA, 1998; p. 380.
24. Fuente, V.; Rufo, L.; Rodríguez, N.; Amils, R.; Zuluaga, J. Metal accumulation screening of the Río Tinto flora (Huelva, Spain). *Biol. Trace Elem. Res.* **2010**, *134*, 318–341. [[CrossRef](#)] [[PubMed](#)]
25. Matinzadeh, Z.; Breckle, S.W.; Mirmassoumi, M.; Akhiani, H. Ionic relationships in some halophytic Iranian Chenopodiaceae and their rizospheres. *Plant Soil* **2013**, *372*, 523–539. [[CrossRef](#)]
26. Álvarez, J.; Alcaraz, F.; Ortiz, R. Soil salinity and moisture gradients and plant zonation in Mediterranean salt marshes of southeast Spain. *Wetlands* **2000**, *20*, 357–372. [[CrossRef](#)]
27. Weiner, S.; Dove, P.M. (Eds.) *Reviews in Mineralogy and Geochemistry*; Mineralogical Society of America: Chantilly, VA, USA, 2003; Volume 54, pp. 1–29.

28. Fraústo da Silva, J.J.R.; Williams, R.J.P. *The Biological Chemistry of the Elements, The Inorganic Chemistry of Life*; Clarendon Press: Oxford, UK, 1991; pp. 467–494.
29. Baran, E.J. *Química Bioinorgánica*, 1st ed.; McGraw Hill Interamericana de España, SL: Madrid, Spain, 1995; pp. 197–212.



© 2018 by the authors. Licensee MDPI, Basel, Switzerland. This article is an open access article distributed under the terms and conditions of the Creative Commons Attribution (CC BY) license (<http://creativecommons.org/licenses/by/4.0/>).